

Terahertz imaging of inhomogeneous electrostatics in single-layer graphene embedded in dielectrics

M. J. Paul,¹ J. L. Tomaino,¹ J. W. Kevek,² T. DeBorde,¹ Z. J. Thompson,¹ E. D. Minot,¹ and Yun-Shik Lee^{1,a)}

¹Department of Physics, Oregon State University, Corvallis, Oregon 97331-6507, USA

²Laboratory of Atomic and Solid-State Physics, Cornell University, Ithaca, New York 14853, USA

(Received 19 June 2012; accepted 17 August 2012; published online 29 August 2012)

We investigate electron transport properties in large-area, single-layer graphene embedded in dielectric media, using free-space terahertz (THz) imaging and time-domain spectroscopy. Sandwiched between a thin polymethyl methacrylate (PMMA) layer and a Si substrate, graphene layers of different growth recipes exhibit distinctive spatial inhomogeneity of sheet conductivity. The non-contacting, non-destructive THz probe reveals that the PMMA layer induces a small, yet noticeable reduction in conductivity. © 2012 American Institute of Physics. [<http://dx.doi.org/10.1063/1.4749280>]

Graphene has a unique band structure including a cone of linear dispersion with its apex at the Dirac point, which gives rise to the extraordinary transport properties of massless relativistic fermions.¹ Charge carriers in a high-quality graphene layer exhibit ultrahigh mobilities, undergoing ballistic transport over a long distance. It has been reported that electron mobilities can exceed $200\,000\text{ cm}^2\text{ V}^{-1}$ in a free-standing graphene device.² The electron mobility in a large-scale graphene sheet, however, suffers a significant reduction ranging from 1000 to $10\,000\text{ cm}^2\text{ V}^{-1}$ ^{3–4} due to scattering with extrinsic sources such as charged impurities^{4–6} and microscopic ripples.^{3,7–9} Dominant scatterers are largely determined by its growth procedure. Furthermore, when a graphene sheet is deposited on a substrate, the symmetry breaking at the interface induces an intrinsic modification of the electronic structure, opening up a band gap at the Dirac point.^{10–14} Inelastic scattering by surface phonons is also considered an underlying mechanism limiting the electron mobility in graphene.^{15–17} Most of the practical graphene devices are fabricated on a substrate providing a supporting structure; thus it is important to understand how the graphene/substrate interface influences the electron dynamics in graphene.

In this letter, we investigate the spatial inhomogeneity of graphene conductivity and the effect of interfaces on conductivity in a graphene sheet embedded between dielectric media using terahertz (THz) imaging and spectroscopy. The THz method utilizes a non-contacting, non-destructive probe to measure the local carrier dynamics of graphene with a high absorption contrast.¹⁸ We measured the transmission of spatially focused, broadband THz pulses through the graphene samples sandwiched by an intrinsic Si substrate and a thin dielectric film of polymethyl methacrylate (PMMA) and mapped out the local sheet conductivity using raster scanning across the samples. Strong THz absorption by graphene ($\sim 20\%$) indicates that intraband transitions dominate the interactions of THz waves with graphene. Graphene samples grown by different recipes show markedly different spatial inhomogeneity of electric conductivity. The addition of a PMMA thin film results in a slight, yet noticeable decrease in the conductivity, while THz absorption by the 100-nm-

thick PMMA film alone (absorption coefficient, $<5\text{ cm}^{-1}$) is negligible. The change in conductivity may be caused by excessive scattering sites and doped carriers at the graphene/PMMA interface.

We grew large-area graphene on copper foil by chemical vapor deposition (CVD). Two types of samples were produced. The first type comes from a standard growth recipe with grain size of $\sim 5\text{ }\mu\text{m}$.¹⁹ The second type was produced using a novel growth technique known as the “pita-pocket method.”²⁰ The grain size of the second type ranges from $50\text{ }\mu\text{m}$ to $400\text{ }\mu\text{m}$. While the individual grain size is larger, the pita-pocket graphene is inhomogeneous in a macroscopic scale of the order of millimeters. An optical microscope image of the pita-pocket graphene on SiO_2 in Fig. 1(a) shows the regions of bare SiO_2 , single-layer graphene, and double-layer graphene, confirmed by Raman spectroscopy [Fig. 1(c)]. After the growth, we deposited a 100-nm-thick PMMA film on graphene. The PMMA/graphene layer was subsequently transferred onto two types of substrates: (1) an intrinsic Si substrate and (2) an intrinsic Si substrate with a 300 nm layer SiO_2 (made for device applications) so that the graphene layer was sandwiched by the two dielectric media.

We employed THz imaging and spectroscopy to investigate the graphene samples. We generated broadband THz pulses (central frequency, 1 THz; bandwidth, 1.5 THz) by optical rectification of femtosecond laser pulses in a 1-mm ZnTe crystal. Our laser system is a 1 kHz Ti:sapphire amplifier (central wavelength, 800-nm; pulse energy, 1 mJ; pulse duration, 90 fs). THz pulses were spatially focused onto the graphene samples with a diffraction limited beam size of 0.5 mm. Figure 1(d) shows a THz transmission geometry used to create two-dimensional raster scan images and perform THz time-domain spectroscopy (THz-TDS). Integrated THz power spectra were measured by a L-He-cooled Si:Bolometer. THz waveforms were measured by electro-optic (EO) sampling with a $150\text{-}\mu\text{m}$ ZnTe crystal.

Figures 2(a) and 2(b) show the THz transmission images of two graphene samples of standard growth and pita-pocket growth. The images cover a $20 \times 20\text{-mm}^2$ region and the pixel size is 0.25 mm. The graphene films shown in dark blue are clearly discernible against the background of the Si substrate (light-blue). The THz response of the standard-growth

^{a)}Electronic mail: leeys@physics.oregonstate.edu.

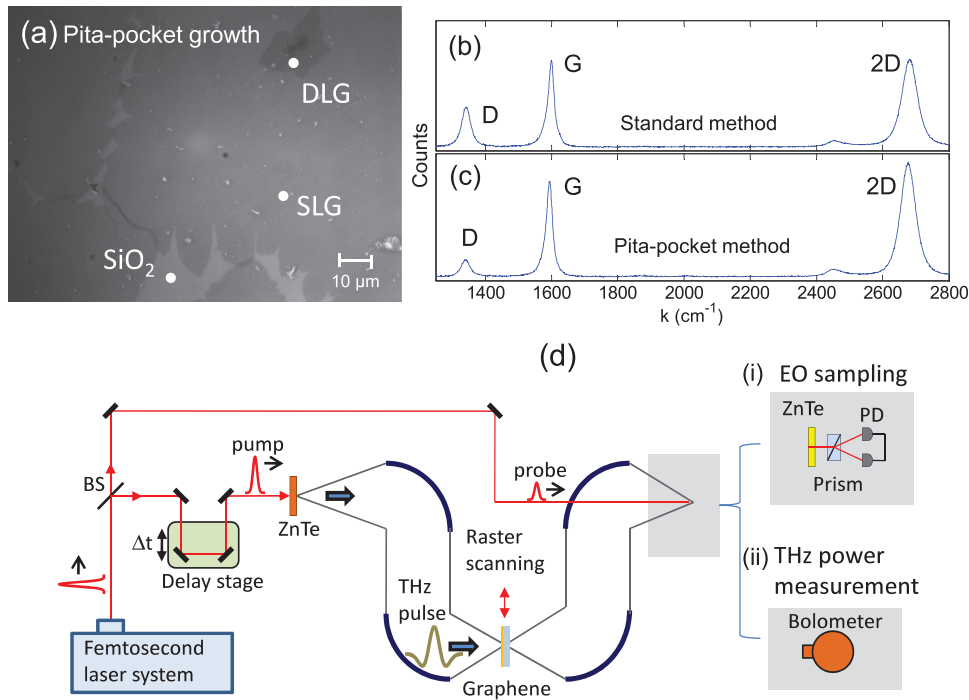


FIG. 1. (a) Optical microscope image (100 \times) of pita-pocket graphene on SiO₂. (b) and (c) Raman spectra of graphene-on-Si with a 300-nm oxide layer: (b) Standard growth sample and (c) pita-pocket growth sample. (d) Schematics of (i) THz time-domain spectroscopy and (ii) raster scan THz imaging.

graphene film is nearly spatially uniform while the pita-pocket-growth film shows strong inhomogeneity. Using the Fresnel thin-film formula based on Drude conductivity, we obtain the local sheet conductivity of graphene (σ_S) via transmission measurements.¹⁸ The transmission of the graphene/Si sample normalized by Si substrate transmission is given as

$$T_{norm} = \left| \frac{t_G}{t_S} \right|^2 \frac{1 - |r_S|^4}{1 - |r_S r_G|^2}, \quad (1)$$

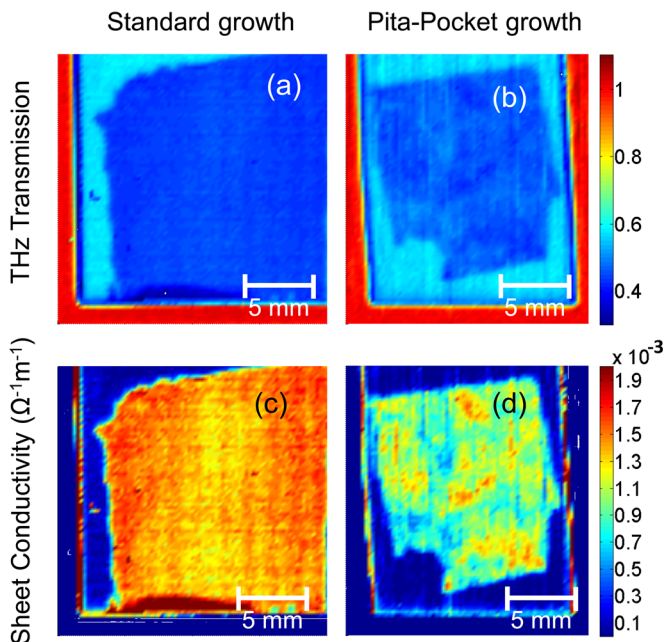


FIG. 2. THz transmission images of the PMMA/graphene/Si samples over a 20 \times 20-mm² region with a 0.25-mm pixel size: (a) standard and (b) pita-pocket growth. The graphene films are shown in dark blue in the light-blue background of the Si substrate. The red regions correspond to air. (c) and (d) show calculated sheet-conductivity σ_S (Ω^{-1}) images over the graphene region.

where t_S (t_G) and r_S (r_G) are transmission and reflection Fresnel coefficients for an air/Si (air/graphene/Si) interface

$$t_G(\sigma_S) = \frac{2}{n_{Si} + 1 + Z_0 \sigma_S},$$

$$r_G(\sigma_S) = \frac{n_{Si} - 1 - Z_0 \sigma_S}{n_{Si} + 1 + Z_0 \sigma_S} \quad (2)$$

with the Si refractive index $n_{Si} = 3.42$ and the vacuum impedance $Z_0 = 376.7 \Omega$. Figures 2(c) and 2(d) show the images of the calculated local sheet-conductivity of the graphene/PMMA layer. The spatial inhomogeneity of the graphene samples is even more pronounced. The local sheet conductivity of the standard-growth graphene exhibits about 10% fluctuation across the sample, $\sigma_S = 1.3 \times 10^{-3}$ to $1.5 \times 10^{-3} \Omega^{-1}$ (sheet resistivity, $\rho_S = 710$ to $830 \Omega/sq$), while that of the pita-pocket growth graphene widely varies from 0.6×10^{-3} to $1.5 \times 10^{-3} \Omega^{-1}$ (sheet resistivity, $\rho_S = 710$ to $1700 \Omega/sq$).

We investigate the effects of PMMA layer on the electron dynamics in graphene, performing THz measurements on both graphene samples, first removing the PMMA layer and then depositing a new PMMA film (thickness, 50 nm). PMMA was removed by an ashing process at 400 $^\circ C$ to ensure an ultraclean surface. This process causes some thermal damage to the standard-growth sample, nearly doubling the D peak in the Raman spectrum. The average sheet conductivity lowers from 1.4×10^{-3} to $0.82 \times 10^{-3} \Omega^{-1}$. On the other hand, the PMMA removal process gives rise to a substantial increase in the average sheet conductivity of the pita-pocket sample from 0.99×10^{-3} to $1.3 \times 10^{-3} \Omega^{-1}$. Figures 3(a)–3(d) show the sheet-conductivity images before and after the new PMMA layer deposition. The average sheet conductivity of the standard-growth (pita-pocket growth) graphene reduces from that of bare graphene-on-Si 0.82×10^{-3} (1.3×10^{-3}) to 0.71×10^{-3} (0.99×10^{-3}) Ω^{-1} . The reduction is uniform across the entire graphene surface.

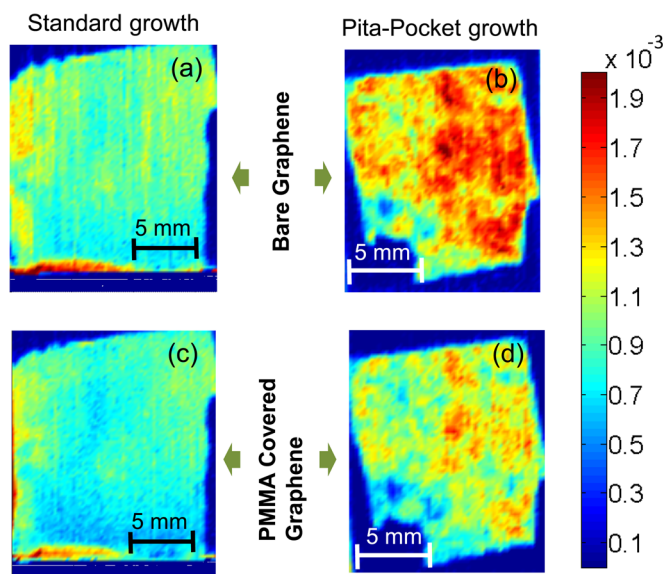


FIG. 3. Sheet conductivity images of the bare and PMMA covered graphene layers. Standard growth: (a) bare and (c) PMMA covered. Pita-pocket growth: (b) bare and (d) PMMA covered.

In order to confirm our analysis based on Drude conductivity, we inspect frequency-dependent conductivity using THz-TDS. When a THz pulse transmitted through the graphene-on-Si sample, a portion of the pulse is directly transmitted, and the remaining portion undergoes multiple internal reflections within the Si substrate. The Si substrate is substantially thick so that the reflected pulses are temporally well separated from each other.¹⁸ Figures 4(a) and 4(b) show directly transmitted THz waveforms through the sample before (red) and after (blue) PMMA deposition. Figures 4(c) and 4(d) show the first internally reflected THz waveform. The solid black line is the THz waveform transmitted through a bare Si substrate. Figure 4(e) shows the relative

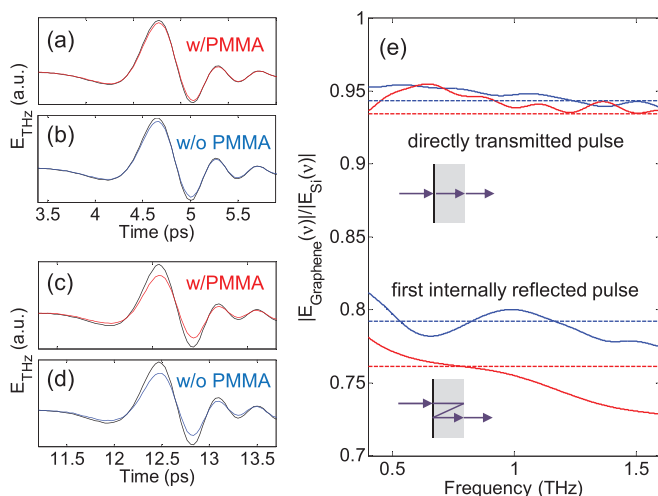


FIG. 4. Transmitted THz waveforms through standard-growth graphene samples: directly transmitted through (a) bare and (c) PMMA covered graphene and first internally reflected through (b) bare and (d) PMMA covered graphene. The thin black lines indicate transmitted pulses through a bare Si substrate. (e) Relative transmission spectra of bare (solid red line) and PMMA covered graphene (solid blue line). The dashed lines at 0.934 (red) and 0.943 (blue) indicate the calculated relative amplitude for the directly transmitted pulse from the measured local sheet conductivity. The dashed lines at 0.761 (red) and 0.792 (blue) are for the first internally reflected pulse.

transmission spectra (the ratio of the electric field transmitted through graphene-on-Si to that through bare Si) before (solid red line) and after (solid blue line) the PMMA deposition. The spectra are nearly flat, indicating the validity of the Drude picture. The THz-TDS results are compared with the calculated values based on the average sheet conductivity (dashed red and blue lines) for both the directly transmitted and first internally reflected pulse.

In conclusion, THz imaging enables non-contact probing of microscopic Drude conductivity in a large-area, single-layer graphene embedded in dielectric media. Graphene samples grown by two different methods show largely different spatial inhomogeneity of the electrical conductivity. A thin PMMA film induces a slight reduction of conductivity in graphene, either through the introduction of additional scattering, a change in doping or a combination of these effects.

This work is supported by the National Science Foundation (DMR-1063632), the Oregon Nanoscience and Microtechnologies Institute, and National Research Foundation of Korea Grant (NRF-2011-220-D00052). We are grateful to Professor Hyunyoung Choi (Yonsei University, Korea) for his expert advice.

- ¹K. S. Novoselov, A. K. Geim, S. V. Morozov, D. Jiang, M. I. Katsnelson, I. V. Grigorieva, S. V. Dubonos, and A. A. Firsov, *Nature* **438**, 197 (2005).
- ²K. I. Bolotin, K. J. Sikes, Z. Jiang, M. Klima, G. Fudenberg, J. Hone, P. Kim, and H. L. Stormer, *Solid State Commun.* **146**, 351 (2008).
- ³S. V. Morozov, K. S. Novoselov, M. I. Katsnelson, F. Schedin, D. C. Elias, J. A. Jaszczak, and A. K. Geim, *Phys. Rev. Lett.* **100**, 016602 (2008).
- ⁴S. Sonde, F. Giannazzo, C. Vecchio, R. Yakimova, E. Rimini, and V. Raineri, *Appl. Phys. Lett.* **97**, 132101 (2010).
- ⁵E. H. Hwang, S. Adam, and S. Das Sarma, *Phys. Rev. Lett.* **98**, 186806 (2007).
- ⁶K. Nomura and A. H. MacDonald, *Phys. Rev. Lett.* **96**, 256602 (2006).
- ⁷M. Ishigami, J. H. Chen, W. G. Cullen, M. S. Fuhrer, and E. D. Williams, *Nano Lett.* **7**, 1643 (2007).
- ⁸F. Schedin, A. K. Geim, S. V. Morozov, E. W. Hill, P. Blake, M. I. Katsnelson, and K. S. Novoselov, *Nature Mater.* **6**, 652 (2007).
- ⁹I. Calizo, W. Bao, F. Miao, C. N. Lau, and A. A. Balandin, *Appl. Phys. Lett.* **91**, 201904 (2007).
- ¹⁰S. Y. Zhou, G.-H. Gweon, A. V. Fedorov, P. N. First, W. A. de Heer, D.-H. Lee, F. Guinea, A. H. Castro Neto, and A. Lanzara, *Nature Mater.* **6**, 770 (2007).
- ¹¹F. Varchon, R. Feng, J. Hass, X. Li, B. N. Nguyen, C. Naud, P. Mallet, J.-Y. Veullen, C. Berger, E. H. Conrad, and L. Magaud, *Phys. Rev. Lett.* **99**, 126805 (2007).
- ¹²G. Giovannetti, P. A. Khomyakov, G. Brocks, P. J. Kelly, and J. van den Brink, *Phys. Rev. B* **76**, 073103 (2007).
- ¹³R. Balog, B. Jørgensen, L. Nilsson, M. Andersen, E. Rienks, M. Bianchi, M. Fanetti, E. Lægsgaard, A. Baraldi, S. Lizzit, Z. Slijivancanin, F. Besenbacher, B. Hammer, T. G. Pedersen, P. Hofmann, and L. Hornekær, *Nature Mater.* **9**, 315 (2010).
- ¹⁴Y. Xu, K. T. He, S. W. Schmucker, Z. Guo, J. C. Koepke, J. D. Wood, J. W. Lyding, and N. R. Aluru, *Nano Lett.* **11**, 2735 (2011).
- ¹⁵J. H. Chen, C. Jang, S. Xiao, M. Ishigami, and M. S. Fuhrer, *Nat. Nanotechnol.* **3**, 206 (2008).
- ¹⁶S. Fratini and F. Guinea, *Phys. Rev. B* **77**, 195415 (2008).
- ¹⁷A. I. Volokitin and B. N. J. Persson, *Phys. Rev. Lett.* **106**, 094502 (2011).
- ¹⁸J. L. Tomaino, A. D. Jameson, J. W. Kevek, M. J. Paul, A. M. van der Zande, R. A. Barton, P. L. McEuen, E. D. Minot, and Y.-S. Lee, *Opt. Express* **19**, 141 (2011).
- ¹⁹X. Li, W. Cai, J. An, S. Kim, J. Nah, D. Yang, R. Piner, A. Velamakanni, I. Jung, E. Tutuc, S. K. Banerjee, L. Colombo, and R. S. Ruoff, *Science* **324**, 1312 (2009).
- ²⁰X. Li, C. W. Magnuson, A. Venugopal, R. M. Tromp, J. B. Hannon, E. M. Vogel, L. Colombo, and R. S. Ruoff, *J. Am. Chem. Soc.* **133**, 2816 (2011).